# Comparative molecular and immunoregulatory analysis of extracellular vesicles from *Candida albicans* and *Candida auris.*

Daniel Zamith-Miranda [1, 2], Heino M. Heyman [3], Sneha P. Couvillion [3], Radames J. B. Cordero [4], Marcio L. Rodrigues [5, 6], Leonardo Nimrichter [6], Arturo Casadevall [4], Rafaela F. Amatuzzi [5], Lysangela R. Alves [5], Ernesto S. Nakayasu [3,*], Joshua D. Nosanchuk [1,2,*]

**Affiliations**

1- Department of Microbiology and Immunology, Albert Einstein College of Medicine, Bronx, New York, USA

2- Division of Infectious Diseases, Department of Medicine, Albert Einstein College of Medicine, Bronx, New York, USA

3- Biological Sciences Division, Pacific Northwest National Laboratory, Richland, Washington, USA

4- Harry Feinstone Molecular Microbiology and Immunology Department, Johns Hopkins Bloomberg School of Public Health, Baltimore, MD, 21205, USA

5- Carlos Chagas Institute, Fundação Oswaldo Cruz (Fiocruz), Curitiba, Brazil

6- Microbiology Institute Paulo de Góes (IMPG), Federal University of Rio de Janeiro, Rio de Janeiro, Brazil

*ESN and JDN share senior authorship

**Correspondence authors**: Ernesto S. Nakayasu (ernesto.nakayasu@pnnl.gov) and Joshua D. Nosanchuk (josh.nosanchuk@einsteinmed.org)

**Keywords**: *Candida auris*, *Candida albicans*, extracellular vesicles, multi-omics, fungal pathogenesis, *candidiasis.*

## Abstract

*Candida auris* is a recently described multidrug-resistant pathogenic fungus that is increasingly responsible for healthcare associated outbreaks across the world. Bloodstream infections of this fungus cause death in up to 70% of the cases. Aggravating this scenario, *C. auris*' disease-promoting mechanisms are poorly understood. Fungi release extracellular vesicles (EVs) carrying a broad range of molecules including proteins, lipids, carbohydrates, pigments, and RNA, many of which are virulence factors. Here, we carried out a comparative molecular characterization of *C. auris* and *C. albicans* EVs and evaluated their capacity to modulate effector mechanisms of host immune defense. Using proteomics, lipidomics, and transcriptomics, we found that *C. auris* released EVs with payloads that were significantly different from EVs released by *C. albicans*. EVs released by *C. auris* potentiated the adhesion of this yeast to an epithelial cell monolayer, while EVs from *C. albicans* had no effect. *C. albicans* EVs primmed macrophages for intracellular yeast killing, whereas *C. auris* EVs promoted survival of the fungal cells. Moreover, EVs from both *C. auris* and *C. albicans* induced the activation of bone marrow-derived dendritic cells. Altogether, our findings show distinct profiles and properties of EVs released by *C. auris* and by *C. albicans,* and highlight the potential contribution of *C. auris* EVs to the pathogenesis of this emerging pathogen.

## Importance

*Candida auris* is a recently described multi-drug resistant pathogenic fungus that is responsible for outbreaks across the globe, particularly in the context of nosocomial infections. Its virulence factors and pathogenesis are poorly understood. In the current work, we tested the hypothesis that extracellular vesicles (EVs) released by *C. auris* is a disease-promoting factor . In this manuscript, we described the production of EVs by *C. auris* and compared their biological activities against the better-characterized EVs from *C. albicans*. *C. auris* EVs have immunoregulatory properties, of which some are opposite of *C. albicans* EVs. We also explored the cargo and structural components of those vesicles and found that they are remarkably distinct than EVs from its phylogenetic relative *Candida albicans*.

## Introduction

*Candida auris* is a recently described pathogenic fungus that has emerged as a serious cause of healthcare associated infections across the world (1). Therefore, it is considered a global threat by the US Center for Disease Control and Prevention (2). The biological challenges for combatting *C. auris* include the fungus' capacity to form resilient biofilms and to resist multiple antifungal drugs (3). *C. auris* kills 30-70% of the infected individuals (4). Although we have deep knowledge regarding the disease-promoting mechanisms deployed by other *Candida* species, relatively little is known about *C. auris*. We have recently compared the molecular profiles of two *C. auris* isolates vs. *Candida albicans* by integrating proteins, lipids, and metabolites of these yeast cells, and demonstrated that *C. auris* has an elevated expression of pathways related to drug resistance and virulence, such as sterol metabolism and drug resistance-related transporters (5).

Disease development is a combination of fungal virulence factors and the affected host's ability to efficiently control the fungal growth, and extracellular vesicles (EVs) play a role in both of these factors. EVs are lipid bilayered structures released by a broad variety of uni- or multicellular organisms (6). Fungal EVs from *Cryptococcus neoformans* were first described in 2007 (7) and they have since been shown as an important mechanism for molecular export in a variety of fungal species. EVs produced by fungi carry many biologically active molecules, including virulence factors and regulators, indicating that they could activate the innate immune system and influence disease development (8-16). *In vitro*, fungal EVs impact phagocyte activity, promoting an increase in cytokine levels, modulating phagocytosis and regulating macrophage polarization (8-10, 14, 16, 17). Together, these data strongly suggest that fungal EVs activate the immune response. Indeed, *Galleria mellonella* larvae are protected by pre-treatment with EVs from *C. albicans*, *C. neoformans* and *Aspergillus flavus* (9, 18, 19). Recently, we demonstrated that immunization of mice with EVs from *C. albicans* confers full protection against systemic candidiasis (11).

However, the outcome of fungal EV and host response depends on the model investigated. For instance, yeast EVs released from co-cultures of dendritic cells (DCs) and *Malassezia sympodialis* induce the production of TNF-□ and higher levels of IL-4 by PBMC from patients with atopic eczema, when compared to control PBMC, displaying an allergic reaction (20, 21). *C. neoformans* and *Sporothrix brasiliensis* EVs are associated with virulence and disease progress in murine models, respectively (22, 23). We hypothesize that the multiple activities attributed to fungal EVs could be dependent on their composition, which at least partially differs according to the species investigated

(9, 21, 24-29). Thus, a more complete analysis on EVs composition could open new views for understanding fungal diseases.

Here, we performed a detailed characterization of EVs released by two distinct strains of *C. auris* (MMC1 and MMC2, which are highly resistant and susceptible to fluconazole, respectively) (5) and *C. albicans*. Differences in size and sterol/protein ratios were observed. Using integrated multi-omics (proteomics, lipidomics and, transcriptomics) analysis we compared EVs and whole cells of *C. auris* and *C. albicans* and demonstrated significant compositional differences that could impact pathogenesis. Developing functional assays, we demonstrated that *C. auris* EVs influence adhesion to epithelial cells and activation of dendritic cells. Together our results show that *C. auris* produces EVs with a distinct composition in comparison with *C. albicans*, and *C. auris* EVs modulate host cell defense mechanisms.

## Methods

**Cell lines**: Two well characterized *C. auris* clinical isolates (MMC1 and MMC2) were acquired from Montefiore Medical Center (NY, USA) (5). *C. albicans* strain (ATCC #90028), RAW 264.7 macrophages (ATTC #TIB-71) and HeLa cells (ATTC #CCL-2) were obtained from ATCC. Yeast cells were cultivated in YPD broth and seeded onto Sabouraud agar plates. For each experiment, colonies were inoculated in Sabouraud broth for 24 h at 30 °C before use. RAW 264.7 and HeLa cell lines were cultivated up to the $10^{th}$ passage in DMEM supplemented with 10% FBS and 1% non-essential amino acids.

**EVs isolation**: One colony of each strain of *C. auris* or *C. albicans* was inoculated in 10 mL of Sabouraud broth for 24 h at 30 °C, and then expanded in 200 mL of fresh medium. After an additional 24 h at 37 °C, the cells were centrifuged. The supernatant was filtered and concentrated 40 fold using an Amicon system with a 100-KDa molecular weight cutoff membrane. The concentrate was centrifuged twice at 150.000 x *g* at 4 ºC for 1 hour, with a PBS washing step between each centrifugation step. The EV pellets were suspended in filtered PBS for most of the experiments, and in 50 mM ammonium bicarbonate for proteomic and lipidomic analyses.

**Transmission Electron Microscopy:** EVs pellets were fixed in 2.5% glutaraldehyde and 3 mM $MgCl_2$ in 0.1 M sodium cacodylate buffer, pH 7.2 overnight at 4 °C. Samples were then rinsed with buffer and post-fixed in 0.8% potassium ferrocyanide reduced 1% osmium tetroxide in the buffer for 1 h on ice in the dark. After a 0.1 M sodium cacodylate buffer rinse, the samples were incubated at 4 °C overnight in the same buffer. Samples were rinsed with 0.1 M maleate buffer, *en bloc* stained with 2% uranyl acetate (0.22 µm filtered, 1 h, dark) in 0.1 M maleate, dehydrated in a graded series of ethanol and embedded in Eponate 12 (Ted PElla) resin. Samples were polymerized at 37 °C for 2 days and at 60 °C overnight. Thin sections, 60 to 90 nm, were cut with a diamond knife on a Reichert-Jung Ultracut E ultramicrotome and picked up with formvar coated copper slot grids. Grids were stained with 2% uranyl acetate in 50% methanol, followed by lead citrate, and observed with a Phillips CM120 transmission electron microscope at 80 kV. Images were captured with an AMT XR80 high-resolution (16-bit) 8 Mpixel camera.

**Protein and ergosterol quantification:** Protein and sterols were quantified using BCA Protein Assay (Thermo) and Amplex Red Cholesterol Assay (Thermo) kits, respectively. Both contents were expressed as a function of the number of yeast cells present in each culture at harvest time.

**Hydrodynamic size distribution of extracellular vesicles by Dynamic light scattering:** EVs were suspended in PBS and their hydrodynamic size distributions were measured in a BI-90 Plus Particle Size Analyzer (Brookhaven Instruments) at room temperature as described (30). Vesicle preparations were first centrifuged at 13,000 rpm for 5 minutes to remove any larger particles and aggregates. One hundred microliters of sample were loaded into disposable cuvette (Eppendorf 952010077) and analyzed by DLS. The average size distribution was calculated from duplicates of ten individual measurements.

**Isolation and sequencing of extracellular vesicles RNAs:** The RNA molecules were isolated with the miRNeasy mini kit (Qiagen) according to the manufacturer's protocol, that enables the purification of molecules from 18 nt up to messenger RNAs. This allowed us to obtain not only the small RNA-enriched fractions but also molecules longer than >200 nt. The RNA profile was assessed in an Agilent 2100 Bioanalyzer (Agilent Technologies). The purified RNA, from three independent biological replicates, was used for RNA-seq library construction using TruSeq small RNA kit (Illumina) according to the manufacturer's recommendations with a slight modification. During the acrylamide gel size selection, we excised the band ranging from 18 nt to >200 nt in length. The sequencing was performed with the Illumina HiSeq 2500 platform, TruSeq SBS Kit v3-HS 50 cycles kit (Illumina).

***In silico* data analysis:** The RNA-seq analysis was performed with CLC Genomics Workbench© software version 20. The *C. auris* B8441 genome used for mapping was obtained from the NCBI database (GCA_002759435.2). The alignment was performed as follows: additional 100-base upstream and downstream sequences; 10 minimum number of reads; 2 maximum number of mismatches; -2 nonspecific match limit, and minimum fraction length of 0.8 for the RNA mapping. The minimum reads similarity mapped on the reference genome was 80%. Only uniquely mapped reads were considered in the analysis. The libraries were normalized per million and the expression values for the transcripts were registered in TPM (Transcripts per Million). For the ncRNA the database used was the ncRNA from the *Candida* genome database: C_auris_B8441_version_sXX-mYY-rZZ_other_features_no_introns.fasta.gz. For the mRNA identification in the EVs, we combined the differential expression with reads coverage, so we performed the map reads to reference (C_auris_B8441_version_s01-m01-r10_genomic and C_auris_B8441_version_s01-m01-r10_other_features_plus_intergenic) using the following parameters: No masking, match score (1), mismatch cost (2), linear insertion cost (3), deletion cost (3), length fraction (0.6), similarity fraction (0.8) and global alignment. To consider the full-length mRNAs we selected those with expression value (TPM) higher than 100 and also 5x transcript coverage. Gene Ontology analysis was performed using the DAVID annotation tool (31).

**Lipidomics and proteomics analyses of extracellular vesicles:** Sample processing and analysis were carried out as described (32, 33). Briefly, samples were submitted to simultaneous Metabolite, Protein and Lipid Extraction (MPLEx) (34). Extracted lipids

were dried in a vacuum centrifuge and dissolved in methanol before analysis by liquid chromatography-tandem mass spectrometry (LC-MS/MS) on a Velos Orbitrap mass spectrometer (Thermo Fisher). Lipid species were identified and manually inspected for validation based on head group and fatty acyl chain fragments using LIQUID (35). The intensities of each lipid species were extracted using MZmine 2.0 (36).

Proteins were dissolved in in 100 µl of 50 mM $NH_4HCO_3$ containing 5 mM dithiothreitol and 8 M urea, and incubated for 15 minutes at 37 °C. Reduced thiol groups were alkylated with a final concentration of 10 mM iodoacetamide (from a 400 mM stock solution) incubated for 30 at room temperature. The reaction was quenched by adding 500 mM dithiothreitol to a final concentration of 20 mM. Samples were diluted 8 fold with 50 mM $NH_4HCO_3$ containing 1 mM $CaCl_2$, and digested with overnight at 37 °C with 2 µg sequencing-grade trypsin (Promega). Samples were desalted with solid-phase extraction C18 spin columns (Ultramicrospin columns, C18, 3- to 30-µg capacity; Nest Group), as previously described (Ref: https://journals.asm.org/doi/epub/10.1128/mSphere.00085-15).

Resulting peptides were dissolved in water and loaded into a C18 trap column (4 cm by 100 µm inner diameter [ID], packed in-house with 5 µm C18; Jupiter). Chromatography was carried out on a capillary column (70 cm x 75 µm ID packed with C18, 3-µm particles) using a gradient of acetonitrile (mobile phase B) in water (mobile phase A), both supplemented with 0.1% formic acid. The elution was carried out at 300 nL/min with the following gradient: 19 min, 8% B; 60 min, 12% B; 155 min, 35% B; 203 min, 60% B; 210 min, 75% B; 215 min, 95% B; 220 min, 95% B. Eluting samples were analyzed online with a Q-Exactive Plus mass spectrometer (Thermo Fisher Scientific).

Full scan spectra were collected in a window of 400 to 2,000 m/z with a resolution of 70,000 at m/z 400. The 12 most intense parent ions were submitted to high-energy collision dissociation (32% normalized collision energy) at a resolution of 17,500. Dynamic exclusion was set to fragment each parent ion once and excluding them for 45 sec.

Peptides were identified using MaxQuant (v.1.5.5.1) (37) by searching against the *C. albicans* SC5314 and *C. auris* sequences from Uniprot Knowledge Base (downloaded December 6, 2017). Intensity-based absolute quantification (iBAQ) method was used for quantification (38). The iBAQ values for individual proteins were normalized against the total sum of all proteins, resulting in the relative protein copy number (percentage from total). *C. auris* and *C. albicans* proteins were considered orthologs with ≥40% amino acid sequence similarity (39). Heatmap and clustering were performed with MultiExperiment Viewer (MeV) (40) or R software and Complex Heatmap package (41). For calculating fold changes and plotting the heatmaps, missing values were filled with half of the minimum value of the dataset. Function-enrichment analysis was done with DAVID (42), using default parameters. Bubble graphs were plot using Minitab v.19.2020.1.

**Adhesion assay to epithelial monolayers:** HeLa cells were seeded on coverslips placed in 24-wells plates and incubated for 24 h at 37 °C. Cell monolayers were pre-incubated with *C. auris* or *C. albicans* EVs (10 µg/mL of protein) for 1 h and challenged with respective yeasts (pre-stained with NHS-Rhodamine for 30 minutes at 30 °C under shaking) for 1 h in a ratio of 20 yeast cells per HeLa cell. NHS-Rhodamine staining does not change yeast cell growth rates or other cellular characteristics (data not shown).

After extensive washing with PBS to remove non-adherent yeast, the cells were fixed with formalin and mounted with mounting media containing DAPI. Images were taken using a fluorescence microscope (Zeiss Imager Z1) and the adhesion was measured by the ratio between NHS-Rhodamine-positive cells divided by DAPI-positive cells for each field, using ImageJ. At least 8 fields containing approximately 400 epithelial cells per field from each slide were counted.

**Analysis of bone marrow-derived dendritic cells (BMDC) activation by extracellular vesicles:** BMDC were differentiated as described (43). Briefly, bone marrow cells were isolated from male C57BL/6 mice (approved protocol #2014-0501) by flushing both tibias and femurs with RPMI supplemented with 10% of fetal bovine serum (FBS). Bone marrow cells were cultivated for 10 days at 37 °C in the presence of GM-CSF (Peprotech) (43). Cultures were fed with media containing GM-CSF at days 3, 6 and 8. BMDC phenotype was evaluated on day 10 by the surface exposure of CD11c and MHCII. At day 10 of differentiation, BMDC were incubated with 1 and 10 µg/mL (protein) of EVs from *C. auris* and *C. albicans* for 24 h at 37 °C and 5% $CO_2$. After this period, cytokines IL-6, IL-10, IL-12p70, TNF-α, and TGF-β were measured in the culture supernatants using ELISA. BMDC were labeled with antibodies (α-CD11c, α-MHCII, α-CD80 and, α-CD86) to evaluate their purity and activation state using flow cytometry.

**Modulation of effector functions of macrophages by extracellular vesicles:**

**Phagocytosis** – RAW 264.7 macrophages were plated onto 96-well plates and incubated for 24 h at 37 ºC. Cells were then incubated with EVs from *C. albicans* or *C. auris* (10 µg/mL of protein) for 1 h until challenge with the respective yeast cell at 1:2 (macrophage : yeast) for 1 h. Plates were washed to remove extracellular yeast cells

and then lysed with sterile water for CFU analysis. **Killing** –Bone marrow cells were harvested from C57BL/6 mice as detailed above and incubated with RPMI medium containing 10% of fetal bovine serum and 20% of L929 supernatant at 37 ºC. On the fourth day, new medium containing L929 supernatant was added to the culture. On the seventh day of cultures, the cells had matured to differentiated macrophages, confirmed by the expression of F4/80 and absence of LY6C. BMDM were plated in 96-well plates and incubated at 37 ºC for 24 h. Cells were incubated with EVs for 4 h at 37 ºC until the challenge with yeast cells at 10:1 (macrophage:yeast) for 24 h at 37 ºC. Cells were lysed and the suspensions plated onto Sabouraud plates for CFU counting.

**Statistical analyses:** All experiments were performed at least 3 independent times, unless stated otherwise. Data sets were analyzed using One-way ANOVA, and Dunnett multi comparison post-test using GraphPad Prism 8. All *p* values lower than 0.05 were considered significant.

## Results

### Morphological characterization of *C. auris* extracellular vesicles

EVs were isolated from the supernatant of *C. albicans* and *C. auris* cultures and then analyzed by transmission electron microscopy (TEM). As reported previously, EVs from *C. albicans* are round and bilayered particles (Figure 1A) (9). Similar results were observed for EVs from both *C. auris* isolates (Figure 1B and 1C), consistent with the reported morphology of other fungal EVs (7, 9, 12, 16, 20, 23, 25, 44). EVs were also analyzed by dynamic light scattering (DLS) to evaluate their global size. The size of EVs

isolated from *C. albicans* and *C. auris* MMC2 were very similar, ranging from 50 and 70 nm and the second population between 170-250 nm (Figure 1A and 1C). *C. auris* MMC1 produced EVs of larger hydrodynamic size, ranging from 100 to 150 and the second population between 280 and 370 nm (Figure 1B).

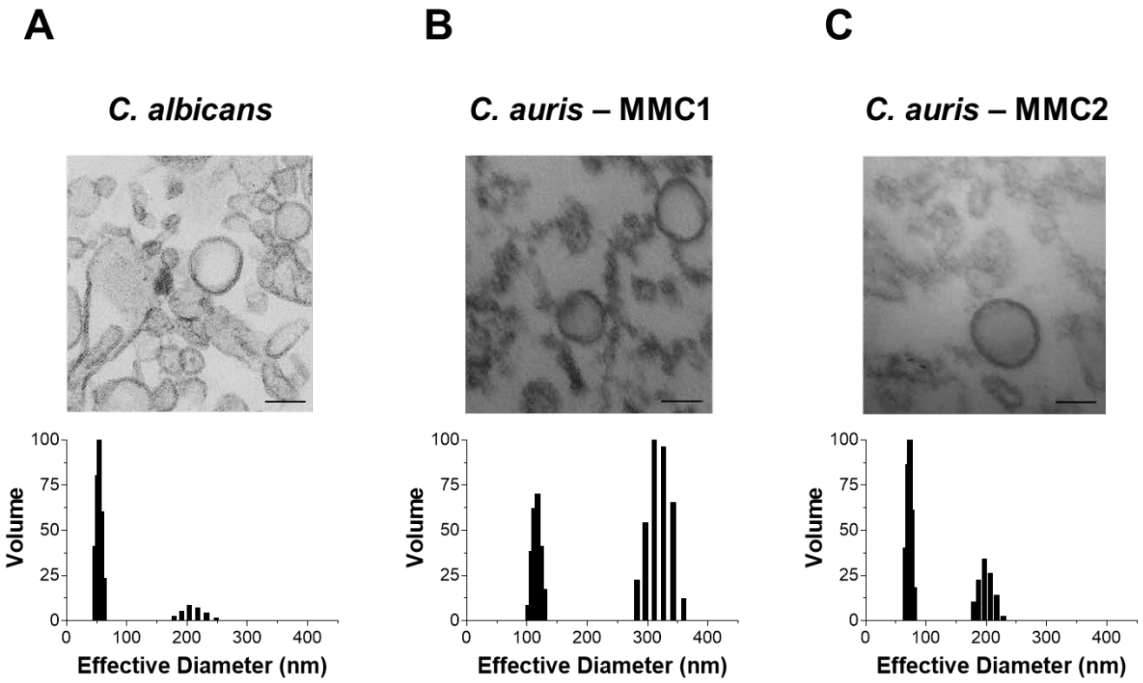


**Figure 1. *C. auris* releases EVs.** Transmission electron micrographs and dynamic light scattering measurements of EVs from *C. albicans* (A) and *C. auris* isolates MMC1 (B) and MMC2 (C). Two independent EVs isolations were analyzed by both methods with similar results. The figure shows representative results of each analysis. Scale bars = 100 nm

**Protein and ergosterol content of *C. auris* extracellular vesicles**

The amount of protein (Fig. 2A) and ergosterol (Fig. 2B) were determined and normalized by the number of yeast cells in culture at the EV harvest time. Both *C. auris* strains secreted similar amounts of protein in EVs, but the amounts were 3-4 times lower compared to *C. albicans*. Likewise, the amounts of EVs ergosterol was 3-6 times lower in *C. auris* strains than in *C. albicans*. *C. auris* MMC2 strain EVs had the lowest amount of ergosterol, being 3 times lower compared to MMC1 (Figure 2B). As ergosterol is a ubiquitous molecule present in EVs membranes, we normalized the protein content by the amount of ergosterol in each strain as a way to measure possible differential protein loads among isolates. MMC2 had a higher protein/ergosterol ratio than either MMC1 or *C. albicans*.

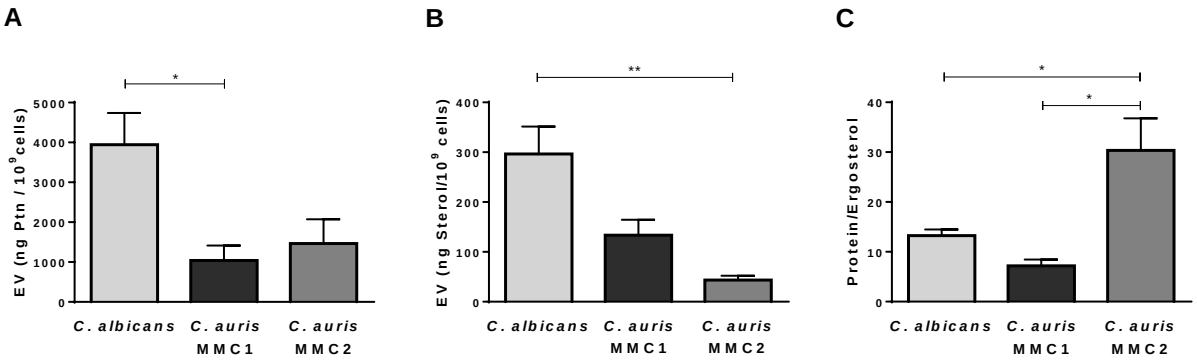


**Figure 2. Protein and sterol content in *C. auris* and *C. albicans* extracellular vesicles (EVs).** Protein (A) and sterol (B) concentrations were measured in EVs suspensions from *C. auris* and *C. albicans* and normalized by the number of cells present in the fungal cultures at the harvest time. (C) Protein to ergosterol concentration ratios. All graphs represent means and standard error of the mean, relative to 4 independent EVs isolations. *p ≤ 0.05; **p ≤ 0.01 by One-way ANOVA followed by Tukey's multiple comparison test.

## RNA content of *C. auris* extracellular vesicles

We performed next-generation sequencing from both MMC1 and MMC2 EVs to investigate their RNA profiles, and compared against *C. albicans* EV-RNA. The analysis was performed applying a minimum of 40% nucleotide similarities between the orthologues. The first observation is that the RNA composition between MMC1 and MMC2 are very similar and most of the molecules identified in *C. auris* EVs were ncRNAs. The most represented ncRNA in *C. auris* in both strains are fragments of tRNAs (Table S1, Figure 3A). In *C. albicans* the tRNAs are also the most represented ncRNAs, and the snoRNAs are the second class of ncRNA in EVs, and this enrichment is not observed in *C. auris* (Figure 3B). For the tRNA fragments there was an enrichment for the 3' or 5' end of the tRNAs however no enrichment in the central portion of the tRNA was observed (Figure S1). Due to the library preparation, in the size selection step we cut the fragments related not only to the small fraction but also longer molecules, allowing the isolation of mRNAs as well. The RNA-seq analysis led to the identification of 57 mRNAs in *C. auris* and 32 in *C. albicans*. The top 10 most abundant transcripts from each species are summarized in Table 1 and all the mRNAs are listed in the Table S2. The transcript antisense to ribosomal RNA, Tar1 was the most enriched in C. *albicans* EVs, followed by the mRNA coding cell division control protein 42 homolog and other transcripts related to cell cycle (Table S2). For *C.auris* the enriched transcripts were peptidyl-prolyl cis-trans isomerase, rapamycin-binding protein, translation elongation factor 1 subunit beta, E3 ubiquitin-activating protein and MFS family membrane transporter (Table S2). To validate the presence of full-length mRNAs

we selected only transcripts with reads coverage greater than 10x. It is possible to observe that we obtained reads mapping along the entire transcript, as for example, the Tar1 mRNA (Figure S2). In addition, it is also possible to observe that the transcript is enriched only in C. *albicans*, no reads are mapping the Tar1 transcript in C. auris MMC1 and MMC2 strains (Figure S2). Overall, our results showed that *C. auris* EV carry RNA, as demonstrated for other fungi (45-47).

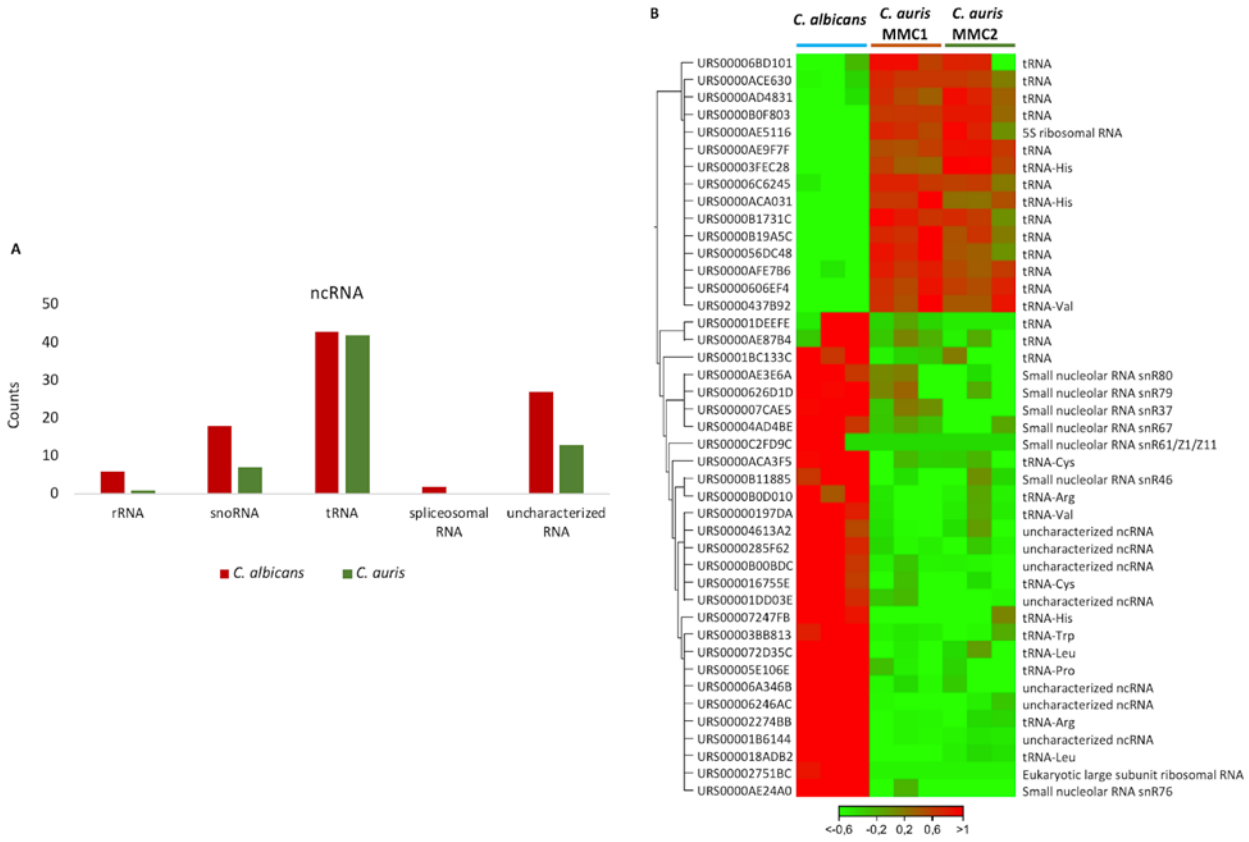


**Figure 3. EV from *C. auris* carry RNA. (A)** Comparison between ncRNAs enriched in the *C. auris* EVs compared *C. albicans* EVs. (B) Heatmap representing the differentially expressed ncRNA in the EVs comparing *C. auris* and *C. albicans* (FDR <1% and fold change FC 10-fold). The expression levels are visualized using a gradient color

scheme, blue – high expression level, red – low expression level and the values represent the logFC.

## Proteomics analysis of extracellular vesicles

We performed a liquid chromatography tandem mass spectrometry (LC-MS/MS)-based proteomic analysis to compare the protein profiles across both species. We utilized a threshold of 40% of homology at amino acid level between the species to consider them homologs (Table S3). The divergent peptide sequences prevent to directly compare peak areas between the two species since the sequence divergency might cause the peptides to not have same signal response in the mass spectrometer. Therefore, we calculated the relative copy number of proteins per sample (% from total) to compare between the two species. In addition to compare the EV proteins from both species, we also compared the EVs data with the proteomics analysis of whole cells (39), which were prepared and run in parallel. We observed striking differences between the whole cells and EVs for each of the 3 strains (Figure 4A). We performed hierarchical clustering to separate groups of proteins based on their abundance profile. Cluster 1, which contains proteins commonly enriched in EVs from *C. auris* and C. *albicans* compared to their respective cells, were enriched in proteins from starch and sucrose metabolism, protein processing in the endoplasmic reticulum, MAP kinases, and amino sugar and nucleotide sugar metabolism (Figure 4A). *C. albicans,* but not *C. auris* EVs, were enriched in abundant cellular proteins, such as ribosomal proteins and proteins from the central carbon and amino acid metabolisms (Cluster 2 in Figure 4A). EVs from both species were depleted of proteins from functions such as ribosomal biogenesis,

proteasome, DNA replication, RNA degradation, and sterol biosynthesis (Clusters 3-5 in Figure 4A). Within the ten most abundant proteins in whole cells, only enolase 1 and pyruvate decarboxylase had high amounts in EVs (*C. albicans*) (Figure 4B). None of the top 10 most abundant whole-cell proteins were abundant in *C. auris* EVs (Figure 4B). On the other hand, the top 10 most abundant EVs proteins were present only in small amounts in whole cells (Figure 4B), suggesting a highly selective process to upload proteins into EVs.

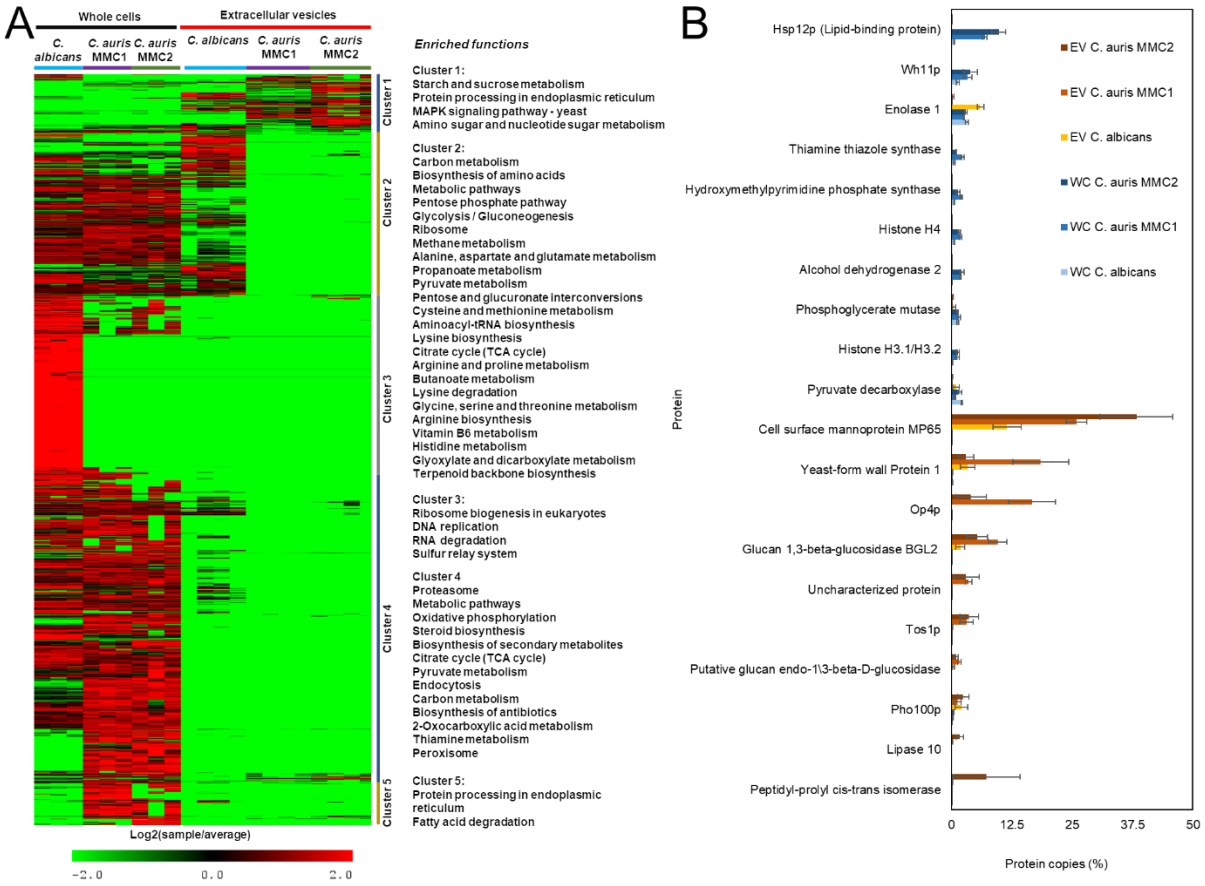


**Figure 4. Comparative proteomic analysis of extracellular vesicles and whole cells from *C. albicans* and *C. auris***. Proteomic data of whole cells and extracellular vesicles were submitted to intensity-based absolute quantification (iBAQ) and converted

to relative copy numbers before comparing across different samples. (A) Heatmaps and hierarchical clustering were performed with MeV and function enrichment of each cluster was performed with DAVID. (B) Profiles of the 10 most abundant whole-cell (WC) and extracellular vesicles (EVs) proteins. Cell samples correspond to three independent cultures and EVs samples correspond to 4 independent EVs isolations.

Among all the proteins detected in EVs, 393 were considered differentially abundant when comparing *C. auris* (both strains) with *C. albicans*. We performed hierarquical clusters of the differential abundant proteins, followed by functional-enrichment analysis. To provide information on the number of proteins in each enriched, we showed the pathway enrichment results as bubble graphs. In this layout, the enrichment fold change and p-values are plot in X and Y axes, respectively, while the circle sizes present the number of proteins and the colors, the clusters they belong to. The number of differentially abundant proteins corresponded to 33% of the detected proteins, so the abundance of the remaining 66% was similar among the species. The heatmap in figure 5A shows all the major differentially abundant EVs proteins among the evaluated organisms. The heatmap was divided into three clusters based on differences of protein abundance between EVs from *C. auris* and *C. albicans*. Out of the 393 proteins on the heatmap, 42 proteins (~10%) were more abundant in *C. auris* than *C. albicans* (Cluster 2, Figure 5). This group of proteins was enriched in proteins from the starch and sucrose metabolism and protein processing in the endoplasmic reticulum (Figure 5B). As mentioned above, *C. albicans* EVs had higher amounts of metabolic proteins (Cluster 3, Figure 5A-B). *C. albicans* EVs had higher amounts of TCA cycle proteins

(figure 5B), which is the opposite of what was found in whole cells (39). This result further supports the presence of a selective mechanism for sorting proteins into the EVs.

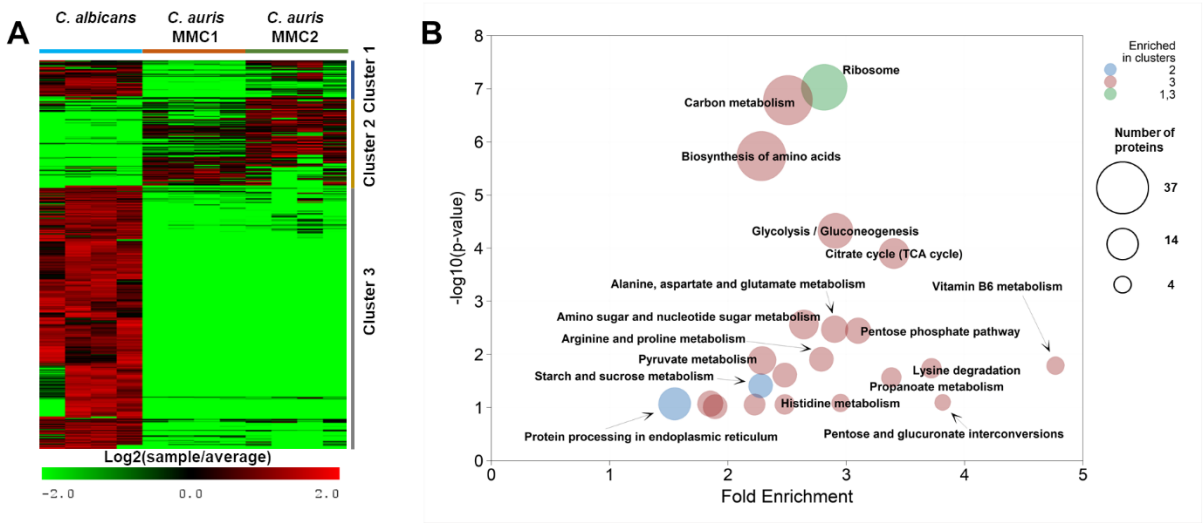


**Figure 5. Proteomics analysis of EVs from *C. auris*.** EVs from both *Candida* species were submitted to protein extraction and analysis. The heatmap (A) shows the abundance of proteins differentially abundant in EVs from both species of *Candida*. The heatmap was clustered using the hierarchical method. (B) Function-enrichment analysis of different clusters of proteins from panel A. The enrichment of pathways was done with DAVID. The graph represents the relationship between p-values and fold enrichment. The colors of the circles represent the different clusters they are enriched in, while the size, the number of proteins from each pathway. EVs samples correspond to 4 independent EVs isolations.

## Lipidomics analysis of extracellular vesicles

We performed a lipidomics analysis to compare the lipid profile of *C. auris* and *C. albicans* EVs (Figure 6A-B). All detected species of diacylglycerols (DG) and triacylglycerols (TG) were more abundant in EVs from *C. albicans*, whereas the majority of glycerophospholipids were enriched in the *C. auris* isolates, including phosphatidylcholine (PC), phosphatidylethanolamine (PE), phosphatidylglycerol (PG) and phosphatidylserine (PS) species (Figure 6A). Conversely, phosphatidic acid (PA) and phosphatidylinositol (PI) species were more abundant in *C. albicans* (Figure 6A). The pattern of sphingolipids was also distinct when the *Candida* EVs were compared. Two major species of conserved hexosylceramides (HexCer) were found in EVs from *C. albicans* and *C. auris* (Figure 6B), corresponding to the same distribution characterized in their respective yeast extracts recently reported by our group (5). Consistent with that, HexCer species bearing Cer(d18:1/24:0(2OH)) and Cer(d20:0/18:0) were more abundant in *C. albicans* EVs. Non-acylated sphingoid bases sphinganine Cer(d18:0/0:0) and sphingosine Cer(d18:1/0:0) were more abundant in *C. auris* MMC2 (Table S4). We also found unusual free ceramide species with acetate as the acyl group (Figure 6C), known as C2-ceramides, which were more abundant in *C. auris* MMC1. Remarkably, Cer(d18:1/2:0) comprises 7.9% of the mass spectrometry signal for all identified lipids in the positive ion mode analysis of *C. auris* MMC1 EVs, but only 0.6% and 0.2% of the *C. auris* MMC2 and *C. albicans* EVs, respectively (Figure 6C). We compared the relative intensities of Cer(d18:1/2:0) to the whole cell data from our recent publication(5). We found an enrichment of 25, 67, and 109 folds of this lipid species in EVs compared to the whole cells in *C. auris* MMC1, *C. auris* MMC2 and *C. albicans*, respectively.

Recently, we reported that *C. auris* had higher expression of a variety of phospholipases compared to *C. albicans* (5), therefore, we took a closer look at their products, lysophospholipids(48). *C. auris* MMC2 EVs had a consistent higher abundance of lysophosphatidylcholine (LPC) and lysophosphatidylethanolamine (LPE) species compared to *C. auris* MMC1 and *C. albicans* (Figure 6D). Lysophosphatidylglycerol (LPG) species, being PG(18:0/0:0), PG(18:1/0:0), and PG(18:2/0:0) more abundant in *C. auris* MMC2, *C. albicans* and *C. auris* MMC1, respectively (Figure 6D).

Fatty acids (FA) chains were detected in all organisms and ranged in size from 14 to 24 carbons, and arachidonic acid was detected, esterified to phosphatidylethanolamine (PE(18:2/20:4)), consistently in both *C. auris* isolates. Arachidonic acid was not abundant in the evaluated strain of *C. albicans* in the tested conditions (Table S4).

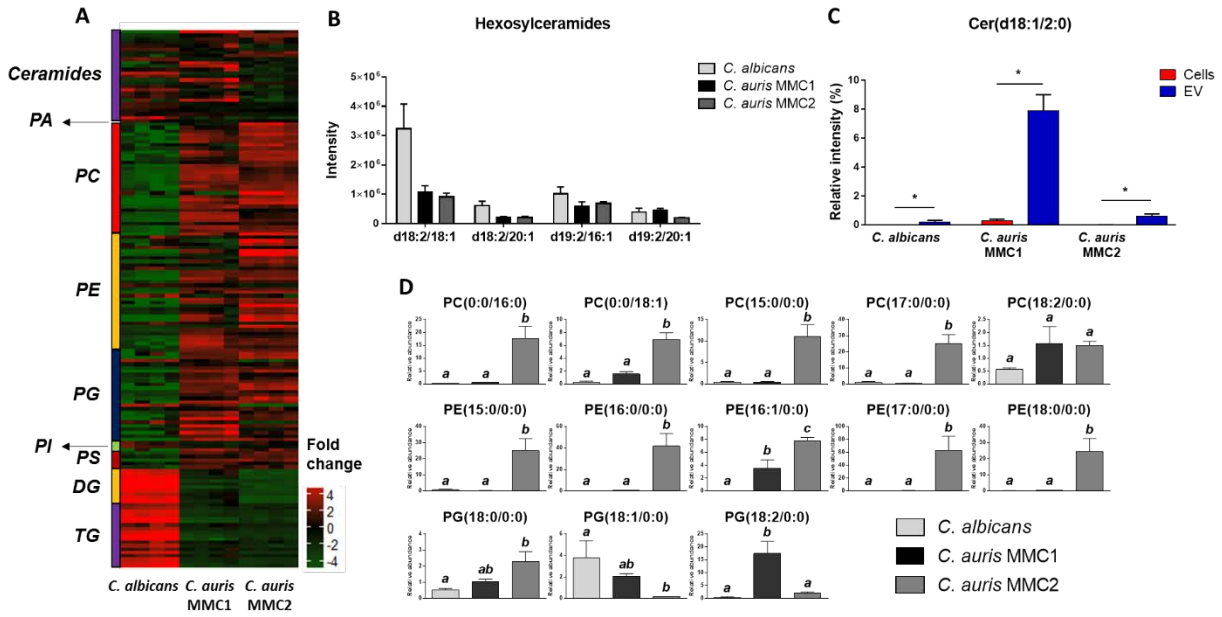


**Figure 6. Lipid profile of *C. auris* and *C. albicans* EVs.** Vesicles from both *Candida* species were submitted to lipid extraction and analysis by LC-MS/MS. (A) Heatmap of

the relative abundances of EVs lipids from both *Candida* species. (B) Relative intensity of hexosylceramides. (C) Relative intensity of Cer(d18:1/2:0) was compared between EVs and yeast cells among all *Candida* species. (D) Relative abundance of lysophospholipids In *C. auris* and *C. albicans* EVs. Data were analyzed by one-way ANOVA followed by Tukey's multiple comparison test. Different letters among bars represent $p < 0.05$. EVs samples correspond to 4 independent EVs isolations.

Abbreviations: Cer, ceramide; DG, diacylglycerol; PA, phosphatidic acid; PC, phosphatidylcholine; PE, phosphatidylethanolamine; PG, phosphatidylglycerol; PI, phosphatidylinositol; PS, phosphatidylserine; TG, triacylglycerol.

**Effects of extracellular vesicles on the yeast adhesion to epithelial cells**

Adhesion to epithelial surfaces is an important feature displayed by pathogenic species of *Candida* as an early stage of colonization of host tissues (49-52). We evaluated whether *C. albicans* or *C. auris* EVs had an impact on the adhesion of *C. auris* or *C. albicans* to HeLa epithelial cells monolayers. Pre-incubation of HeLa cells with *C. auris* MMC1 EVs increased the adhesion of this yeast. The same was not seen for MMC2 or for *C. albicans,* as the pre-treatment with their EVs did not affect the adhesion of yeast to HeLa cells (Figure 7). This result shows how EVs from different strains of the same species can induce distinct host cells phenotypes.

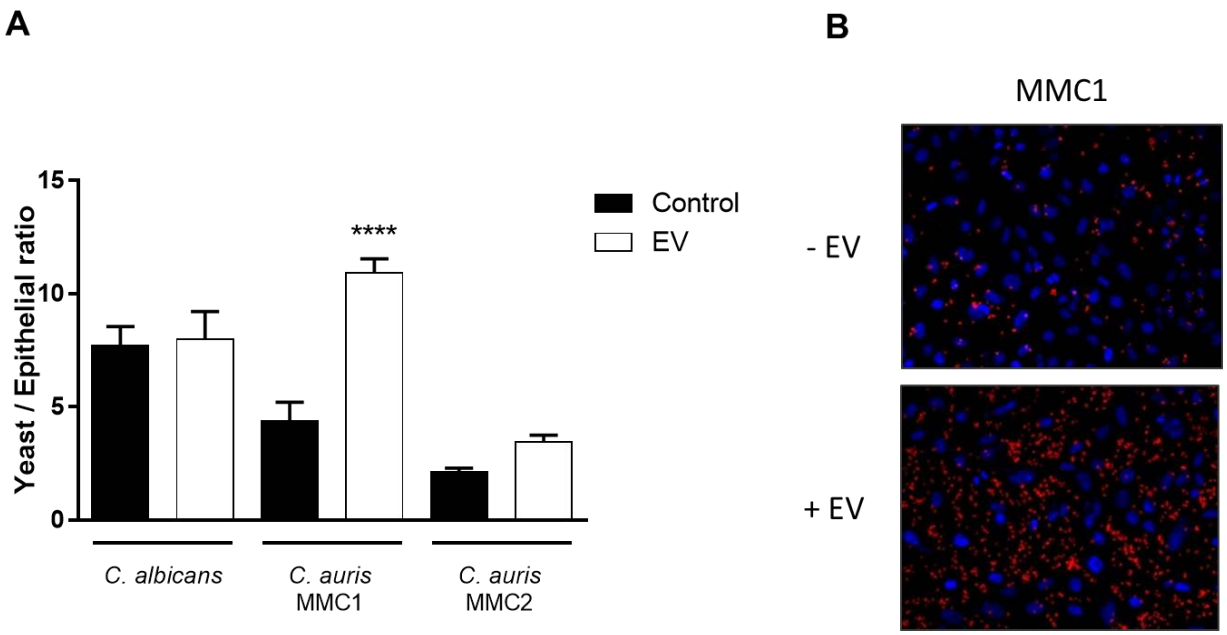


**Figure 7. The effect of extracellular vesicle (EVs) pretreatment on the adhesion of yeast cells to epithelial monolayers**. HeLa cells were pre-treated, or not, with EVs (10 µg/mL of protein) for 1 h before challenging with the respective yeast cells. After incubating for 1 h, monolayers were washed, and slides were analyzed under a fluorescence microscope (see Methods for details). (A) Quantification of adhering yeast cells. (B) Fluorescence image of *C. auris* MMC1 adhesion to HeLa cells. Nuclei were stained with DAPI (blue), whereas the yeasts were stained with NHS-Rhodamine (red). The graph shows average and standard errors relative to 2 independent experiments made with distinct EV preparations. *$p < 0.05$ by one-way ANOVA followed by Dunnet test.

**Effect of extracellular vesicles on phagocytosis and killing by macrophages**

EVs from certain fungi can affect the way yeast cells are internalized and killed by macrophages (8, 13-16, 53). We tested whether EVs from *C. auris* or *C. albicans* would be able to modulate the uptake or clearance of yeast cells by macrophages. The incubation with EVs from either *C. albicans* or *C. auris* had no significant effect on the phagocytosis of yeast cells by macrophages (Figure 8A). However, whereas EVs pre-incubation enhanced macrophages' ability to kill *C. albicans*, EVs from *C. auris* MMC2 but not MMC1, enhanced yeast cell proliferation within the macrophages (Figure 8B). This points to differing roles for EVs among species regarding some of the effector functions of macrophages.

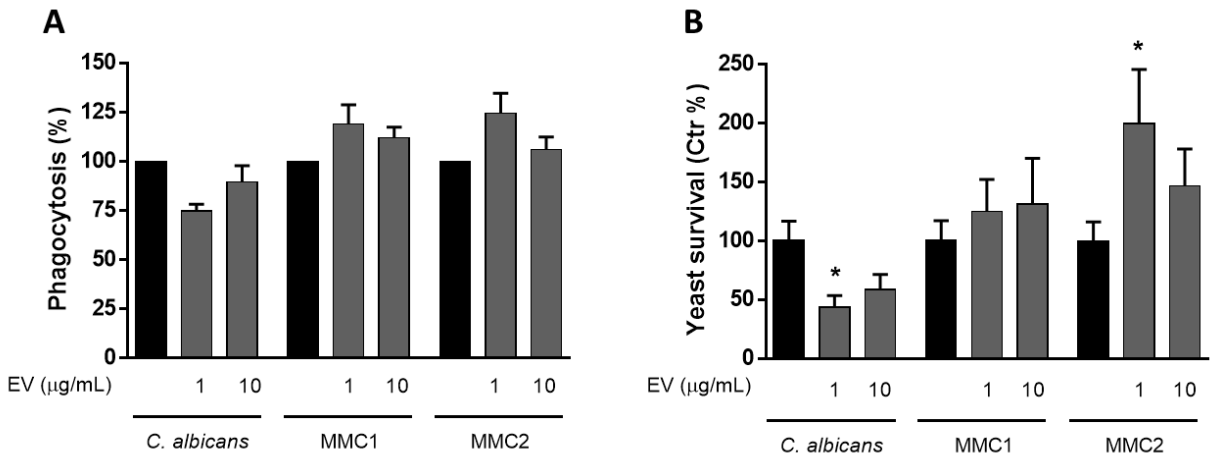


**Figure 8. Phagocytosis and killing by macrophages**. (A) RAW 264.7 macrophages were incubated with EVs for 1 h and then challenged with yeast cells in the ratio of 1:2 (macrophage:yeast) for 1 h. After this period, extracellular yeast cells were washed off and macrophages were lysed and plated onto Sabouraud for CFU counting. (B) Bone marrow-derived macrophages were incubated with EVs for 4 h and then challenged with yeast in the ratio of 10:1 (macrophages:yeast) for 24 h. The macrophages were then lysed and plated onto Sabouraud for CFU counting. Graphs show averages and

493 standard error on the mean for 4 independent experiments made with distinct EV
494 preparations. *$p < 0.05$ by paired T-test.

495

496 **Activation of dendritic cells by extracellular vesicles**

497 We investigated the ability of *C. auris* to regulate dendritic cells by measuring 3
498 important signals for antigen presentation and activation of T cells, MHC-II, co-
499 stimulatory molecules (CD80 and CD86), and cytokines (54). BMDC were incubated for
500 24 h with *C. auris* or *C. albicans* EVs, and MHC-II and co-stimulatory molecules were
501 measured by FACS, whereas cytokines were assayed by ELISA. We observed an
502 increase of surface markers associated with BMDC activation, which was similar to the
503 one induced by LPS. Despite that, MMC2 EVs induced a lower response, and all tested
504 EVs concentrations from *C. auris* and *C. albicans* were able to increase, in a dose-
505 dependent manner, the expression of MHCII, CD80, and CD86 on BMDC (Figure 9A-
506 C). BMDC treated with EVs from both *Candida* species did not produce IL-10, IL-12 or
507 TNF-α. However, BMDC stimulated with EVs from *C. auris* produced IL-6 similarly to *C.*
508 *albicans* (Figure 9D). In addition, inhibition of the basal production of TGF-β by BMDC
509 was detected after the incubation with EVs from *C. auris* MMC1 and *C. albicans* (Figure
510 9E).

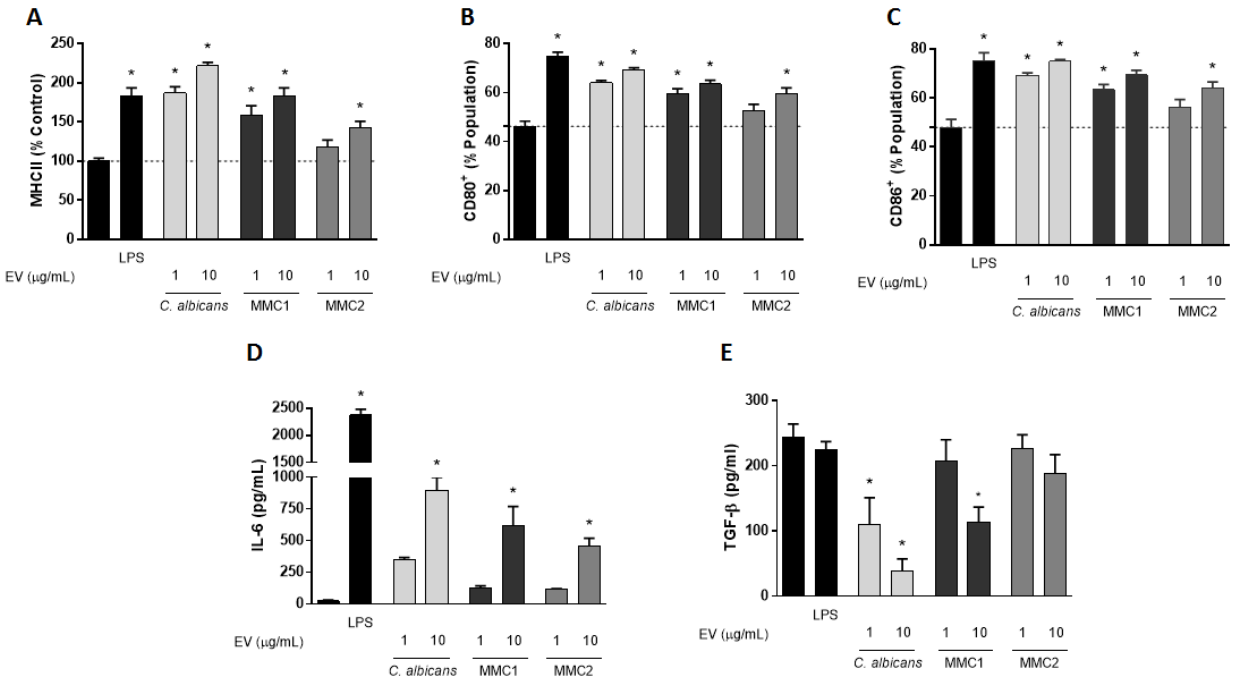


511

512 **Figure 9. Activation of BMDC by *C. auris* extracellular vesicles (EVs).** BMDC were
513 incubated, or not with EVs from *C. albicans* and *C. auris* for 24 h and then analyzed by
514 flow cytometry (A-C) for the expression of MHC-II (A), CD80 (B) and CD86, or ELISA
515 (7D and 7E), for the production of IL-6 (D) and TGF-β (E). Graphs show mean and
516 standard error for 3 independent experiments made with distinct EV preparations. * = p
517 < 0.05 by ANOVA followed by Tukey.

518

519 **Discussion**

520 The literature reports two distinct populations of EVs from other species of *Candida*, a
521 smaller one ranging usually from 50-70 nm, and a larger group between 100 and 800
522 nm (9, 25, 44). We found that *C. auris* releases EVs encompassed by lipid bilayers with
523 size and shape consistent with those from other species. TEM showed that, as opposed

to some species such as *Histoplasma capsulatum* (25) and *Cryptococcus neoformans* (24), *C. auris* EVs lack electron-dense areas associated with pigmentation. The total content of protein and ergosterol in EVs suspensions was higher in *C. albicans* than in either *C. auris* strain when normalized by the number of producing cells. The ratio between proteins and sterol excludes the number of cells from the analysis and *C. auris* MMC2 had a ratio higher than *C. albicans* or *C. auris* MMC1.

EVs RNAs have been characterized in *C. neoformans*, *S. cerevisiae*, *P. brasiliensis*, *H. capsulatum* and *C. albicans* (45, 46). The most abundant transcripts of EVs from *C. auris* MMC1 and MMC2 were associated with general metabolism, ribonuclease, and ubiquitin activities or from uncharacterized genes. EVs mRNAs of *C. albicans* and *C. auris* share common biological processes, such as cellular response to stress and filamentous growth, indicating a conserved sorting mechanism (45). In other eukaryotes, EVs mRNAs can be translated into the recipient cell (55), although this should be experimentally addressed for fungal EVs. The most abundant ncRNAs in EVs from *C. auris* MMC1 and MMC2 were tRNAs and their fragments, similar to previously described for *C. albicans* (~60%). These fragments of tRNA have been described in EVs of diverse organisms, from unicellular parasites to human cells (56-58). In T lymphocytes-derived EVs, the most abundant class of RNA characterized is tRNA fragments, comprising 45% of all RNA identified in the EVs compared to the cell content, and these fragments act by repressing immune activation in T cells (59).

The EVs proteomic profile was strikingly different from the cells they are derived from. Whereas *C. auris* EVs were enriched in proteins from the starch and sucrose metabolism and protein processing in the endoplasmic reticulum, *C. albicans* EVs had

higher amounts of proteins from the central carbon metabolism, ribosomes, and amino acid metabolism. We have previously shown that TCA cycle proteins were more abundant in *C. auris* yeast cells than *C. albicans* (39), but we are now showing an opposite phenotype in EVs, suggesting a selective sorting that could help control the intracellular levels of specific metabolic enzymes. These differences suggest that the EVs from *C. albicans* and *C. auris* are involved with distinct metabolic adaptations. In terms of lipid composition, the relative abundance of lipids involved with energy storage, as triacyl- and diacylglycerols (TG and DG), is remarkably higher in EVs from *C. albicans*, when compared to the *C. auris* ones, reflecting the pattern found in their originating yeast cells (5). The relative abundance of structural glycerophospholipids is consistently higher in EVs from both isolates of *C. auris*, also reflecting the lipid profile of their generating yeast cells (5). Although for some cases the lipid profile from *C. auris* EVs resembled the yeast cell one, some lipids from the yeast cells were not present in EVs, such as cardiolipins, which are mitochondrial markers. The amount of HexCer correlated with the distribution in their respective cells, as previously showed by our group (5). Considered initially as membrane structural components, HexCer were described as virulence regulators in *C. albicans* and *C. neoformans* (60, 61). Their role in EVs could be linked to membrane and lipid raft stability (62). However, recently, Xisto and colleagues demonstrated that purified HexCer produced by the opportunistic fungus *Lomentospora prolificans* induced an oxidative burst by and increased the antifungal activity of macrophages (63).

To our knowledge, our findings report the first time that a C2-ceramide derivative has been found in fungal EVs. In mammalian models, C2-ceramide has biological properties

such as antitumoral activity inducing apoptosis and arresting cell cycle (64, 65). The relative abundance of lysophospholipids was considerably higher in EVs from *C. auris* than *C. albicans*, particularly in EVs from MMC2. This data suggests an intense activity of lipid catabolic enzymes in *C. auris*, such as phospholipases. Some lysophospholipids are biologically active on leukocytes, for instance, LPC released by apoptotic neutrophils recruit monocytes from the bloodstream to promote clearance of apoptotic bodies from tissues (66). Immunomodulatory properties of LPC were demonstrated for other infection models and LPC could act as a virulence factor in *C. auris* infections (67, 68).

To examine the potential biological effects of EVs upon host cells and to compare biological activities between species, we used amounts of EVs based on protein concentration in the same range as used in other reports for host-pathogen studies (8, 9, 16, 17). Within this concentration range, EVs from other pathogenic fungi, were proven to be biologically active in distinct models. Adhesion of yeast cells to epithelial surfaces is an important mechanism of disease as an initial step for further tissue damage and colonization of distinct sites in the host, including the bloodstream (52). *C. albicans* can interact with surface adhesion molecules on epithelial cells (50, 51), so we investigated whether EVs from both *Candida* species were able to modulate the adhesion of yeast to epithelial monolayers *in vitro*. Although the tested strains were able to adhere to the epithelial monolayer, a significant increase in adhesion was observed when EVs from *C. auris* MMC1 were added to the monolayer. Notably, *C. neoformans* EVs fuse with brain microvascular endothelial cells, changing their permeability (22). Since in our studies the epithelial cells were incubated with EVs prior to the challenge

593 with yeast cells, it is possible that fusion with the epithelial cells could modify their
594 permeability and/or modulate the exposure of adhesion molecules, although further
595 experimentation is needed to address this hypothesis. Molecules involved with the
596 adhesion of *C. albicans* to epithelial cells have been described, such as *C. albicans*
597 ALs3p and Eap1p, and are potential players in the increase of adhesion induced by EVs
598 (69).

599 Fungal EVs can induce the activation of phagocytes, increasing phagocytosis, cytokine
600 production, and antigen presentation (8-10, 17). EVs isolated from both *C. auris* strains
601 did not modulate the uptake of yeast cells by macrophage cell lines as RAW, but EVs
602 from *C. auris* MMC2 inhibited the killing of yeast cells by BMDM. EVs from *C. albicans*
603 increased the killing of yeast cells by BMDM. EVs from other pathogenic fungi can
604 modulate phagocytosis and/or killing by macrophages, but our data shows that EVs
605 from only one of the *C. auris* isolates (MMC2) could inhibit the killing of the pathogen by
606 macrophages. This data suggests that EVs from the same species could promote
607 distinct changes in host cells. EVs from *C. albicans* followed the pattern played by most
608 fungal EVs, as they induced killing (8, 10, 14-16, 53). The incubation with EVs
609 stimulated BMDC to express important signals responsible for CD4+ T cells activation
610 such as MHCII, CD80 and CD86. The secretion of TNF-α, IL-10 and IL-12p70 by BMDC
611 was not detected at biologically relevant levels. However, EVs from both *C. albicans*
612 and *C. auris* induced the release of IL-6 by BMDC, while decreasing the basal
613 production of TGF-β. This suggests that EVs from *C. albicans* and *C. auris* MMC1
614 induce an inflammatory response in BMDC. Apart from previously reported (9), TNF-α,
615 IL-10 and IL-12p70 were not produced by BMDC stimulated with EVs. Different strain of

*C. albicans* were used these studies, reinforcing the possibility that the biological activity of EVs could be strain specific.

In summary, our results show that the emerging pathogen *C. auris* produces EVs that are similar in size to other pathogenic fungi, but the content of these EVs distinctly differs from what is known for *C. albicans* and these differences could explain the phenotypic changes induced by these EVs in the cells from the host. In this regard, we note that *C. auris* is a new fungal pathogen that has been proposed to have emerged from the environment as a result of global warming (70). In contrast, *C. albicans* has an ancient association with human hosts. Thus, the similarities in structure and content between *C. auris* and *C. albicans* EVs probably reflect constraints common to fungal cells and their physiology, while the differences reflect species-specific variables and perhaps the result of differences in the time of adaptation to human hosts.

**Acknowledgements**

The Johns Hopkins University School of Medicine Microscope Facility. D.Z.M., J.D.N. and E.S.N. were supported by National Institute of Health-National Institute of Allergy and Infectious Diseases R21 AI124797. L.N. was supported by grants from the Brazilian agency Conselho Nacional de Desenvolvimento Científico e Tecnológico (CNPq, grants 311179/2017-7 and 408711/2017-7) and FAPERJ (E-26/202.809/2018). M.L.R. was supported by grants from the Brazilian Ministry of Health (grant number 440015/2018-9), Conselho Nacional de Desenvolvimento Científico e Tecnológico (CNPq, grants 405520/2018-2, and 301304/2017-3) and Fiocruz (grants PROEP-ICC 442186/2019-

3, VPPCB-007- FIO-18 and VPPIS-001-
FIO18). M.L.R. also acknowledges support from the Instituto Nacional de Ciência e Tecnologia de Inovação em Doenças de Populações Negligenciadas (INCT-IDPN). A.C. was supported in part by NIH grants AI052733, AI15207 and HL059842. Parts of this work were performed in the Environmental Molecular Science Laboratory, a U.S. Department of Energy (DOE) national scientific user facility at PNNL in Richland, WA.

## References

1. Snyder GM, Wright SB. 2019. The Epidemiology and Prevention of Candida auris. Current Infectious Disease Reports 21:19.
2. Li W, Hu Y. 2017. Assessment of Post-Vaccination Phagocytic Activation Using Candida albicans Killing Assays. Methods Mol Biol 1625:313-326.
3. Kean R, Ramage G. 2019. Combined Antifungal Resistance and Biofilm Tolerance: the Global Threat of Candida auris. mSphere 4.
4. Rhodes J, Fisher MC. 2019. Global epidemiology of emerging Candida auris. Current Opinion in Microbiology 52:84-89.
5. Zamith-Miranda D, Heyman HM, Cleare LG, Couvillion SP, Clair GC, Bredeweg EL, Gacser A, Nimrichter L, Nakayasu ES, Nosanchuk JD. 2019. Multi-omics Signature of *Candida auris*, an Emerging and Multidrug-Resistant Pathogen. mSystems 4:e00257-19.
6. Rodrigues ML, Godinho RMC, Zamith-Miranda D, Nimrichter L. 2015. Traveling into Outer Space: Unanswered Questions about Fungal Extracellular Vesicles. PLOS Pathogens 11:e1005240.
7. Rodrigues ML, Nimrichter L, Oliveira DL, Frases S, Miranda K, Zaragoza O, Alvarez M, Nakouzi A, Feldmesser M, Casadevall A. 2007. Vesicular polysaccharide export in Cryptococcus neoformans is a eukaryotic solution to the problem of fungal trans-cell wall transport. Eukaryot Cell 6:48-59.
8. Oliveira DL, Freire-de-Lima CG, Nosanchuk JD, Casadevall A, Rodrigues ML, Nimrichter L. 2010. Extracellular vesicles from Cryptococcus neoformans modulate macrophage functions. Infect Immun 78:1601-9.
9. Vargas G, Rocha JD, Oliveira DL, Albuquerque PC, Frases S, Santos SS, Nosanchuk JD, Gomes AM, Medeiros LC, Miranda K, Sobreira TJ, Nakayasu ES, Arigi EA, Casadevall A, Guimaraes AJ, Rodrigues ML, Freire-de-Lima CG, Almeida IC, Nimrichter L. 2015. Compositional and immunobiological analyses of extracellular vesicles released by Candida albicans. Cell Microbiol 17:389-407.

10. da Silva TA, Roque-Barreira MC, Casadevall A, Almeida F. 2016. Extracellular vesicles from Paracoccidioides brasiliensis induced M1 polarization in vitro. Sci Rep 6:35867.
11. Vargas G, Honorato L, Guimarães AJ, Rodrigues ML, Reis FCG, Vale AM, Ray A, Nosanchuk JD, Nimrichter L. Protective effect of fungal extracellular vesicles against murine candidiasis. Cellular Microbiology n/a:e13238.
12. Vallejo MC, Matsuo AL, Ganiko L, Medeiros LC, Miranda K, Silva LS, Freymuller-Haapalainen E, Sinigaglia-Coimbra R, Almeida IC, Puccia R. 2011. The pathogenic fungus Paracoccidioides brasiliensis exports extracellular vesicles containing highly immunogenic alpha-Galactosyl epitopes. Eukaryot Cell 10:343-51.
13. Almeida F, Wolf JM, da Silva TA, DeLeon-Rodriguez CM, Rezende CP, Pessoni AM, Fernandes FF, Silva-Rocha R, Martinez R, Rodrigues ML, Roque-Barreira MC, Casadevall A. 2017. Galectin-3 impacts Cryptococcus neoformans infection through direct antifungal effects. Nat Commun 8:1968.
14. Brauer VS, Pessoni AM, Bitencourt TA, de Paula RG, de Oliveira Rocha L, Goldman GH, Almeida F. 2020. Extracellular Vesicles from *Aspergillus flavus* Induce M1 Polarization *In Vitro*. mSphere 5:e00190-20.
15. Bitencourt TA, Rezende CP, Quaresemin NR, Moreno P, Hatanaka O, Rossi A, Martinez-Rossi NM, Almeida F. 2018. Extracellular Vesicles From the Dermatophyte Trichophyton interdigitale Modulate Macrophage and Keratinocyte Functions. Frontiers in Immunology 9: .
16. Souza JAM, Baltazar LdM, Carregal VM, Gouveia-Eufrasio L, de Oliveira AG, Dias WG, Rocha de Miranda K, Malavazi I, Santos DdA, Frézard FJG, de Souza DdG, Teixeira MM, Soriani FM. 2019. Characterization of Aspergillus fumigatus Extracellular Vesicles and Their Effects on Macrophages and Neutrophils Functions. Frontiers in Microbiology 10.
17. Baltazar LM, Zamith-Miranda D, Burnet MC, Choi H, Nimrichter L, Nakayasu ES, Nosanchuk JD. 2018. Concentration-dependent protein loading of extracellular vesicles released by Histoplasma capsulatum after antibody treatment and its modulatory action upon macrophages. Scientific Reports 8:8065.
18. Colombo AC, Rella A, Normile T, Joffe LS, Tavares PM, de SAGR, Frases S, Orner EP, Farnoud AM, Fries BC, Sheridan B, Nimrichter L, Rodrigues ML, Del Poeta M. 2019. Cryptococcus neoformans Glucuronoxylomannan and Sterylglucoside Are Required for Host Protection in an Animal Vaccination Model. mBio 10.
19. Brauer VS, Pessoni AM, Bitencourt TA, de Paula RG, de Oliveira Rocha L, Goldman GH, Almeida F. 2020. Extracellular Vesicles from Aspergillus flavus Induce M1 Polarization In Vitro. mSphere 5.
20. Gehrmann U, Qazi KR, Johansson C, Hultenby K, Karlsson M, Lundeberg L, Gabrielsson S, Scheynius A. 2011. Nanovesicles from Malassezia sympodialis and Host Exosomes Induce Cytokine Responses – Novel Mechanisms for Host-Microbe Interactions in Atopic Eczema. PLOS ONE 6:e21480.
21. Johansson HJ, Vallhov H, Holm T, Gehrmann U, Andersson A, Johansson C, Blom H, Carroni M, Lehtio J, Scheynius A. 2018. Extracellular nanovesicles

released from the commensal yeast Malassezia sympodialis are enriched in allergens and interact with cells in human skin. Sci Rep 8:9182.
22. Huang SH, Wu CH, Chang YC, Kwon-Chung KJ, Brown RJ, Jong A. 2012. Cryptococcus neoformans-derived microvesicles enhance the pathogenesis of fungal brain infection. PLoS One 7:e48570.
23. Ikeda MAK, de Almeida JRF, Jannuzzi GP, Cronemberger-Andrade A, Torrecilhas ACT, Moretti NS, da Cunha JPC, de Almeida SR, Ferreira KS. 2018. Extracellular Vesicles From Sporothrix brasiliensis Are an Important Virulence Factor That Induce an Increase in Fungal Burden in Experimental Sporotrichosis. Frontiers in Microbiology 9.
24. Rodrigues ML, Nakayasu ES, Oliveira DL, Nimrichter L, Nosanchuk JD, Almeida IC, Casadevall A. 2008. Extracellular vesicles produced by Cryptococcus neoformans contain protein components associated with virulence. Eukaryot Cell 7:58-67.
25. Albuquerque PC, Nakayasu ES, Rodrigues ML, Frases S, Casadevall A, Zancope-Oliveira RM, Almeida IC, Nosanchuk JD. 2008. Vesicular transport in Histoplasma capsulatum: an effective mechanism for trans-cell wall transfer of proteins and lipids in ascomycetes. Cell Microbiol 10:1695-710.
26. Vallejo MC, Nakayasu ES, Matsuo AL, Sobreira TJ, Longo LV, Ganiko L, Almeida IC, Puccia R. 2012. Vesicle and vesicle-free extracellular proteome of Paracoccidioides brasiliensis: comparative analysis with other pathogenic fungi. J Proteome Res 11:1676-85.
27. Gil-Bona A, Llama-Palacios A, Parra CM, Vivanco F, Nombela C, Monteoliva L, Gil C. 2015. Proteomics unravels extracellular vesicles as carriers of classical cytoplasmic proteins in Candida albicans. J Proteome Res 14:142-53.
28. Matos Baltazar L, Nakayasu ES, Sobreira TJ, Choi H, Casadevall A, Nimrichter L, Nosanchuk JD. 2016. Antibody Binding Alters the Characteristics and Contents of Extracellular Vesicles Released by Histoplasma capsulatum. mSphere 1.
29. Zhao K, Bleackley M, Chisanga D, Gangoda L, Fonseka P, Liem M, Kalra H, Al Saffar H, Keerthikumar S, Ang C-S, Adda CG, Jiang L, Yap K, Poon IK, Lock P, Bulone V, Anderson M, Mathivanan S. 2019. Extracellular vesicles secreted by Saccharomyces cerevisiae are involved in cell wall remodelling. Communications Biology 2:305.
30. Eisenman HC, Frases S, Nicola AM, Rodrigues ML, Casadevall A. 2009. Vesicle-associated melanization in Cryptococcus neoformans. Microbiology 155:3860-7.
31. Huang DW, Sherman BT, Lempicki RA. 2009. Systematic and integrative analysis of large gene lists using DAVID bioinformatics resources. Nature Protocols 4:44-57.
32. Nakayasu ES, Nicora CD, Sims AC, Burnum-Johnson KE, Kim Y-M, Kyle JE, Matzke MM, Shukla AK, Chu RK, Schepmoes AA, Jacobs JM, Baric RS, Webb-Robertson B-J, Smith RD, Metz TO. 2016. MPLEx: a Robust and Universal Protocol for Single-Sample Integrative Proteomic, Metabolomic, and Lipidomic Analyses. mSystems 1:e00043-16.
33. Coelho C, Brown L, Maryam M, Vij R, Smith DFQ, Burnet MC, Kyle JE, Heyman HM, Ramirez J, Prados-Rosales R, Lauvau G, Nakayasu ES, Brady NR,

Hamacher-Brady A, Coppens I, Casadevall A. 2019. Listeria monocytogenes virulence factors, including listeriolysin O, are secreted in biologically active extracellular vesicles. Journal of Biological Chemistry 294:1202-1217.
34. Nakayasu ES, Nicora CD, Sims AC, Burnum-Johnson KE, Kim YM, Kyle JE, Matzke MM, Shukla AK, Chu RK, Schepmoes AA, Jacobs JM, Baric RS, Webb-Robertson BJ, Smith RD, Metz TO. 2016. MPLEx: a Robust and Universal Protocol for Single-Sample Integrative Proteomic, Metabolomic, and Lipidomic Analyses. mSystems 1.
35. Kyle JE, Crowell KL, Casey CP, Fujimoto GM, Kim S, Dautel SE, Smith RD, Payne SH, Metz TO. 2017. LIQUID: an-open source software for identifying lipids in LC-MS/MS-based lipidomics data. Bioinformatics 33:1744-1746.
36. Pluskal T, Castillo S, Villar-Briones A, Oresic M. 2010. MZmine 2: modular framework for processing, visualizing, and analyzing mass spectrometry-based molecular profile data. BMC Bioinformatics 11:395.
37. Cox J, Mann M. 2008. MaxQuant enables high peptide identification rates, individualized p.p.b.-range mass accuracies and proteome-wide protein quantification. Nat Biotechnol 26:1367-72.
38. Schwanhausser B, Busse D, Li N, Dittmar G, Schuchhardt J, Wolf J, Chen W, Selbach M. 2011. Global quantification of mammalian gene expression control. Nature 473:337-42.
39. Zamith-Miranda D, Heyman HM, Cleare LG, Couvillion SP, Clair GC, Bredeweg EL, Gacser A, Nimrichter L, Nakayasu ES, Nosanchuk JD. 2019. Multi-omics Signature of Candida auris, an Emerging and Multidrug-Resistant Pathogen. mSystems 4.
40. Howe EA, Sinha R, Schlauch D, Quackenbush J. 2011. RNA-Seq analysis in MeV. Bioinformatics 27:3209-10.
41. Gu Z, Eils R, Schlesner M. 2016. Complex heatmaps reveal patterns and correlations in multidimensional genomic data. Bioinformatics 32:2847-2849.
42. Huang da W, Sherman BT, Lempicki RA. 2009. Bioinformatics enrichment tools: paths toward the comprehensive functional analysis of large gene lists. Nucleic Acids Res 37:1-13.
43. Lutz MB, Kukutsch N, Ogilvie ALJ, Rößner S, Koch F, Romani N, Schuler G. 1999. An advanced culture method for generating large quantities of highly pure dendritic cells from mouse bone marrow. Journal of Immunological Methods 223:77-92.
44. Karkowska-Kuleta J, Kulig K, Karnas E, Zuba-Surma E, Woznicka O, Pyza E, Kuleta P, Osyczka A, Rapala-Kozik M, Kozik A. 2020. Characteristics of Extracellular Vesicles Released by the Pathogenic Yeast-Like Fungi Candida glabrata, Candida parapsilosis and Candida tropicalis. Cells 9:1722.
45. Peres da Silva R, Puccia R, Rodrigues ML, Oliveira DL, Joffe LS, Cesar GV, Nimrichter L, Goldenberg S, Alves LR. 2015. Extracellular vesicle-mediated export of fungal RNA. Sci Rep 5:7763.
46. Alves LR, Peres da Silva R, Sanchez DA, Zamith-Miranda D, Rodrigues ML, Goldenberg S, Puccia R, Nosanchuk JD. 2019. Extracellular Vesicle-Mediated RNA Release in *Histoplasma capsulatum*. mSphere 4:e00176-19.

47. Peres da Silva R, Longo LGV, Cunha JPCd, Sobreira TJP, Rodrigues ML, Faoro H, Goldenberg S, Alves LR, Puccia R. 2019. Comparison of the RNA Content of Extracellular Vesicles Derived from Paracoccidioides brasiliensis and Paracoccidioides lutzii. Cells 8:765.
48. Barman A, Gohain D, Bora U, Tamuli R. 2018. Phospholipases play multiple cellular roles including growth, stress tolerance, sexual development, and virulence in fungi. Microbiological Research 209:55-69.
49. Wachtler B, Wilson D, Haedicke K, Dalle F, Hube B. 2011. From attachment to damage: defined genes of Candida albicans mediate adhesion, invasion and damage during interaction with oral epithelial cells. PLoS One 6:e17046.
50. Maza PK, Bonfim-Melo A, Padovan ACB, Mortara RA, Orikaza CM, Ramos LMD, Moura TR, Soriani FM, Almeida RS, Suzuki E, Bahia D. 2017. Candida albicans: The Ability to Invade Epithelial Cells and Survive under Oxidative Stress Is Unlinked to Hyphal Length. Frontiers in Microbiology 8.
51. Mikamo H, Yamagishi Y, Sugiyama H, Sadakata H, Miyazaki S, Sano T, Tomita T. 2018. High glucose-mediated overexpression of ICAM-1 in human vaginal epithelial cells increases adhesion of Candida albicans. J Obstet Gynaecol 38:226-230.
52. Moyes DL, Richardson JP, Naglik JR. 2015. Candida albicans-epithelial interactions and pathogenicity mechanisms: scratching the surface. Virulence 6:338-346.
53. Bielska E, Sisquella MA, Aldeieg M, Birch C, O'Donoghue EJ, May RC. 2018. Pathogen-derived extracellular vesicles mediate virulence in the fatal human pathogen Cryptococcus gattii. Nat Commun 9:1556.
54. Romani L. 2011. Immunity to fungal infections. Nat Rev Immunol 11:275-88.
55. Kim KM, Abdelmohsen K, Mustapic M, Kapogiannis D, Gorospe M. 2017. RNA in extracellular vesicles. WIREs RNA 8:e1413.
56. Lambertz U, Oviedo Ovando ME, Vasconcelos EJR, Unrau PJ, Myler PJ, Reiner NE. 2015. Small RNAs derived from tRNAs and rRNAs are highly enriched in exosomes from both old and new world Leishmania providing evidence for conserved exosomal RNA Packaging. BMC Genomics 16:151.
57. Garcia-Silva MR, Cura das Neves RF, Cabrera-Cabrera F, Sanguinetti J, Medeiros LC, Robello C, Naya H, Fernandez-Calero T, Souto-Padron T, de Souza W, Cayota A. 2014. Extracellular vesicles shed by Trypanosoma cruzi are linked to small RNA pathways, life cycle regulation, and susceptibility to infection of mammalian cells. Parasitology Research 113:285-304.
58. Garcia-Silva MR, Cabrera-Cabrera F, das Neves RF, Souto-Padron T, de Souza W, Cayota A. 2014. Gene expression changes induced by Trypanosoma cruzi shed microvesicles in mammalian host cells: relevance of tRNA-derived halves. Biomed Res Int 2014:305239.
59. Chiou N-T, Kageyama R, Ansel KM. 2018. Selective Export into Extracellular Vesicles and Function of tRNA Fragments during T Cell Activation. Cell Reports 25:3356-3370.e4.
60. Noble SM, French S, Kohn LA, Chen V, Johnson AD. 2010. Systematic screens of a Candida albicans homozygous deletion library decouple morphogenetic switching and pathogenicity. Nature Genetics 42:590-598.

61. Rittershaus PC, Kechichian TB, Allegood JC, Merrill AH, Hennig M, Luberto C, Del Poeta M. 2006. Glucosylceramide synthase is an essential regulator of pathogenicity of Cryptococcus neoformans. The Journal of Clinical Investigation 116:1651-1659.
62. Raj S, Nazemidashtarjandi S, Kim J, Joffe L, Zhang X, Singh A, Mor V, Desmarini D, Djordjevic J, Raleigh DP, Rodrigues ML, London E, Del Poeta M, Farnoud AM. 2017. Changes in glucosylceramide structure affect virulence and membrane biophysical properties of Cryptococcus neoformans. Biochimica et Biophysica Acta (BBA) - Biomembranes 1859:2224-2233.
63. Xisto MIDdS, Henao JEM, Dias LdS, Santos GMP, Calixto RdOR, Bernardino MC, Taborda CP, Barreto-Bergter E. 2019. Glucosylceramides From Lomentospora prolificans Induce a Differential Production of Cytokines and Increases the Microbicidal Activity of Macrophages. Frontiers in Microbiology 10.
64. Ahn EH, Yang H, Hsieh C-Y, Sun W, Chang C-C, Schroeder JJ. 2019. Evaluation of chemotherapeutic and cancer-protective properties of sphingosine and C2-ceramide in a human breast stem cell derived carcinogenesis model. Int J Oncol 54:655-664.
65. Chou H-L, Lin Y-H, Liu W, Wu C-Y, Li R-N, Huang H-W, Chou C-H, Chiou S-J, Chiu C-C. 2019. Combination Therapy of Chloroquine and C2-Ceramide Enhances Cytotoxicity in Lung Cancer H460 and H1299 Cells. Cancers 11:370.
66. Peter C, Waibel M, Radu CG, Yang LV, Witte ON, Schulze-Osthoff K, Wesselborg S, Lauber K. 2008. Migration to Apoptotic “Find-me” Signals Is Mediated via the Phagocyte Receptor G2A. Journal of Biological Chemistry 283:5296-5305.
67. Silva-Neto MA, Lopes AH, Atella GC. 2016. Here, There, and Everywhere: The Ubiquitous Distribution of the Immunosignaling Molecule Lysophosphatidylcholine and Its Role on Chagas Disease. Front Immunol 7:62.
68. Tounsi N, Meghari S, Moser M, Djerdjouri B. 2015. Lysophosphatidylcholine exacerbates Leishmania major-dendritic cell infection through interleukin-10 and a burst in arginase1 and indoleamine 2,3-dioxygenase activities. International Immunopharmacology 25:1-9.
69. Moyes DL, Richardson JP, Naglik JR. 2015. Candida albicans-epithelial interactions and pathogenicity mechanisms: scratching the surface. Virulence 6:338-46.
70. Casadevall A, Kontoyiannis DP, Robert V. 2019. On the Emergence of Candida auris: Climate Change, Azoles, Swamps, and Birds. mBio 10.

**Table 1. Gene ontology for RNAs enriched in EVs from *C. auris* and *C. albicans***

## *C. auris*

| Name | Protein names | TPM mean | $Log_2$ fold change | FDR p-value |
|---|---|---|---|---|
| CAALFM_C109220WA | MFS domain-containing protein | **1112.50** | **6.50** | **0.00%** |

| | | | | |
|---|---|---|---|---|
| CAALFM_C112570CA | Elongator subunit | **1357.63** | **6.63** | **0.00%** |
| CAALFM_C207040WA | HIT-type domain-containing protein | **953.50** | **4.06** | **0.06%** |
| POX18 | Pox18p | **809.32** | **6.06** | **0.00%** |
| CAALFM_C111080WA | 6-phosphofructo-2-kinase | **494.49** | **2.87** | **1.39%** |
| RBP1 | FK506-binding protein 1 (FKBP) (EC 5.2.1.8) (Peptidyl-prolyl cis-trans isomerase) (PPIase) (Rapamycin-binding protein) | **1586.55** | **8.36** | **0.00%** |
| MET1 | Uroporphyrinogen-III C-methyltransferase | **1103.00** | **3.23** | **0.05%** |
| STE24 | CAAX prenyl protease (EC 3.4.24.84) | **422.40** | **5.87** | **0.00%** |
| RGS2 | GTPase-activating protein | **507.00** | **6.58** | **0.00%** |
| CAALFM_C204870CA | THO complex subunit 2 | **238.36** | **5.07** | **0.00%** |
| CAALFM_C114310WA | Deoxycytidine monophosphate deaminase | **842.16** | **7.38** | **0.00%** |
| RGS2 | GTPase-activating protein | **507.00** | **6.58** | **0.00%** |

## *C. albicans*

| Name | Protein names | TPM mean | $Log_2$ fold change | FDR p-value |
|---|---|---|---|---|
| TAR1 | Tar1p | **14740.21** | **-14.32** | **0.00%** |
| CDC42 | Cell division control protein 42 homolog | **2280.43** | **-3.90** | **0.01%** |
| THR4 | Threonine synthase (EC 4.2.3.1) | **1486.19** | **-5.44** | **0.00%** |
| THS1 | Threonyl-tRNA synthetase (EC 6.1.1.3) | **1624.40** | **-5.15** | **0.00%** |
| PHHB | 4a-hydroxytetrahydrobiopterin dehydratase (EC 4.2.1.96) | **1763.12** | **-6.29** | **0.00%** |
| CAALFM_CR02690WA | CAP-Gly domain-containing protein | **753.92** | **-4.94** | **0.00%** |
| CAALFM_C107850CA | Anaphase promoting complex subunit | **1198.57** | **-3.16** | **0.26%** |
| GCN20 | Putative AAA family ATPase | **1083.26** | **-3.31** | **0.05%** |
| CAALFM_C501410CA | ER membrane protein complex subunit 1 | **392.62** | **-3.33** | **0.01%** |
| POM152 | Pom152p | **390.75** | **-3.55** | **0.00%** |
| MRPL8 | Mitochondrial 54S ribosomal protein YmL8 | **559.14** | **-4.39** | **0.00%** |
| CAALFM_C100200CA | RRM domain-containing protein | **341.91** | **-3.17** | **0.00%** |